



Polarization-selective enhancement of Nd³⁺ photoluminescence assisted by linear chains of silver nanoparticles

E. Yraola^a, L. Sánchez-García^a, C. Tserkezis^b, P. Molina^a, M.O Ramírez^a,
J. Aizpurua^b, L.E. Bausá^{a,*}

^a Departamento Física de Materiales and Instituto Nicolás Cabrera, Universidad Autónoma de Madrid, 28049 Madrid, Spain

^b Center for Materials Physics (CSIC-UPV/EHU) and Donostia International Physics Center (DIPC), Paseo Manuel Lardizabal 4, 20018 Donostia/San Sebastián, Spain

ARTICLE INFO

Article history:

Received 22 November 2014

Accepted 23 December 2014

Available online 1 January 2015

Keywords:

Luminescence enhancement

Nd³⁺ emission

Linear chain of metal nanoparticles

Localized surface plasmons

Boundary-element calculation

ABSTRACT

A control of the emission of Nd³⁺ ions by polarization-dependent plasmon modes, supported by chains of silver nanoparticles deposited on the surface of a Nd³⁺:LiNbO₃ crystal, is demonstrated. By combining micro-fluorescence measurements with theoretical calculations based on the boundary-element method, we explain how the energy splitting between the longitudinal and transverse modes of silver nanoparticle chains produces a selective enhancement of the Nd³⁺ emission Stark lines: exciting radiative modes of silver nanoparticle chains with light polarized parallel to their axis produces a spectral-selective intensification of the π -character Stark transitions of Nd³⁺ located in the vicinity of the silver nanoparticles. The results are relevant to the design of devices for coherent generation at the nanoscale based on rare earth solid state gain media.

© 2015 Elsevier B.V. All rights reserved.

1. Introduction

The manipulation of light-matter interaction phenomena at the nanoscale by means of plasmonic nanostructures is currently a subject of an intense activity from both fundamental and technological points of view [1,2]. Noble metal nanostructures exhibit the capability to couple light with the collective oscillations of their conduction-band electrons, which can result into a strong confinement of the electromagnetic field in the vicinity of the metallic physical boundaries. This can be used to enhance the interactions between far-field light and optical emitters placed in close proximity with the metallic nanostructures [1,3].

Recently, some of the authors have shown the interest of combining the optical response of metallic nanostructures with optically active ferroelectric materials. Using a photochemical procedure, periodic distributions of silver nanoparticles (Ag NPs) were selectively assembled on polar and non-polar surfaces (Z- and Y-cut, respectively) of a Nd³⁺-doped periodically-poled LiNbO₃ (PPLN) ferroelectric laser crystal in which laser action and coherent self-frequency converted radiation were demonstrated [4]. Photochemical assembly of Ag metallic NPs showed domain-specific deposition as well as a preferential formation of chains of Ag NPs on the surface of the 180° ferroelectric domain boundaries [5,6]. By

exploiting the unique features of plasmonic nanostructures, an enhancement of both the second harmonic generation and the luminescence of Nd³⁺ ions took place when the metallic NPs were deposited on a Nd³⁺ doped PPLN crystal [7]. In addition, due to the linear character of the Ag NPs arrangement, a strong polarization dependence of the photoluminescence of Nd³⁺ ions emitting in the vicinity of the Ag NPs, was observed [8].

Here, we get deeper insight into the analysis of the polarization-selective enhancement of the photoluminescence of Nd³⁺ ions around the chains of Ag NPs. By combining spatially resolved spectroscopic measurements with theoretical calculations based on the boundary-element method (BEM), we show and explain the relationship between the polarization-sensitive radiative plasmonic modes supported by finite chains of silver NPs and the selective enhancement of the π polarized Nd³⁺ emission in the uniaxial LiNbO₃ crystal.

The manuscript is structured as follows. First, the polarized spectra of the collective plasmonic modes associated with Ag NPs distributed in long linear chains are calculated taking into account both the NP size and the separation distance distributions in our crystal. Second, the results from dark field microscopy are related to the calculated scattering cross-section spectra of the chains of Ag NPs. The polarized absorption spectra of Nd³⁺ ions are experimentally obtained in the spectral region overlapping the main mode of the Ag NPs. Finally, the influence of the polarization of the plasmon resonance supported by linear chains of Ag NPs on the optical properties of Nd³⁺ ions in this solid state gain medium is analyzed by means of the ⁴F_{3/2} → ⁴I_{11/2} emission of Nd³⁺ ions. As

* Corresponding author.

E-mail address: luisa.bausa@uam.es (L.E. Bausá).

will be shown, exciting the chain of NPs with light polarized parallel to its axis produces a spectral selection of the π -character Stark transitions of Nd^{3+} ions located in the vicinity of the Ag NPs. The results are of interest in the search for efficient subwavelength confinement and active control of light at nanoscale dimensions in rare earth based solid state gain media.

2. Materials and methods

2.1. Materials and synthesis

Nd^{3+} doped PPLN crystals were grown by the off-centered Czochralski method along the x -axis by adding Nd (1 mol %) in the form of Nd_2O_3 . A 1 mm thick plate was cut and polished with its main faces oriented parallel to the ferroelectric c -axis (Y-cut).

The photoinduced silver deposition process was carried out by illuminating the surface of the Y-cut PPLN crystal with above-band gap light provided by a mercury lamp (main line at 253.6 nm) while the crystal was immersed in a 0.01 M AgNO_3 solution at 70 °C. The power of the lamp was $5400 \mu\text{W cm}^{-2}$ at a distance of 3 cm. The illumination time was 10 min. Further details on the experimental procedure can be found elsewhere [5,6]. A scanning electron microscope (SEM) model Philips XL30 SFEQ was used to obtain the nanometric-scaled images of the metallic nanoparticles.

2.2. Optical measurements

Dark field microscopy was performed in transmission configuration by using an Olympus BX51 microscope equipped with a dark-field condenser.

Far-field micro-luminescence experiments were performed with a laser scanning confocal microscope provided with a two-axis XY motorized platform with 0.1 μm spatial resolution controlled by software. An Ar^+ laser (Spectra Physics Model 177-Series) with a filtered emission at 488 nm was used as excitation source. The laser

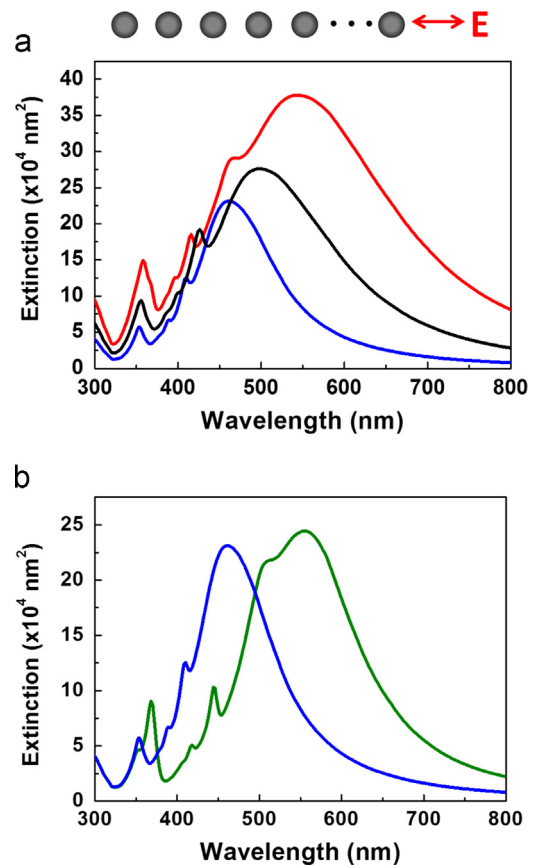


Fig. 2. Calculated extinction cross-section spectra of different linear chains of 15 Ag NPs for a plane wave polarized along the chain axis; (a) Effect of the nanoparticle size: (blue) 50 nm diameter, (red) 70 nm diameter, (black) mixed chain with 6 NPs of 70 nm and 9 NPs of 50 nm. (b) Effect of the inter-particle distance: (blue) 5 nm, (green) 2 nm. For interpretation of the references to color in this figure legend, the reader is referred to the web version of this article.

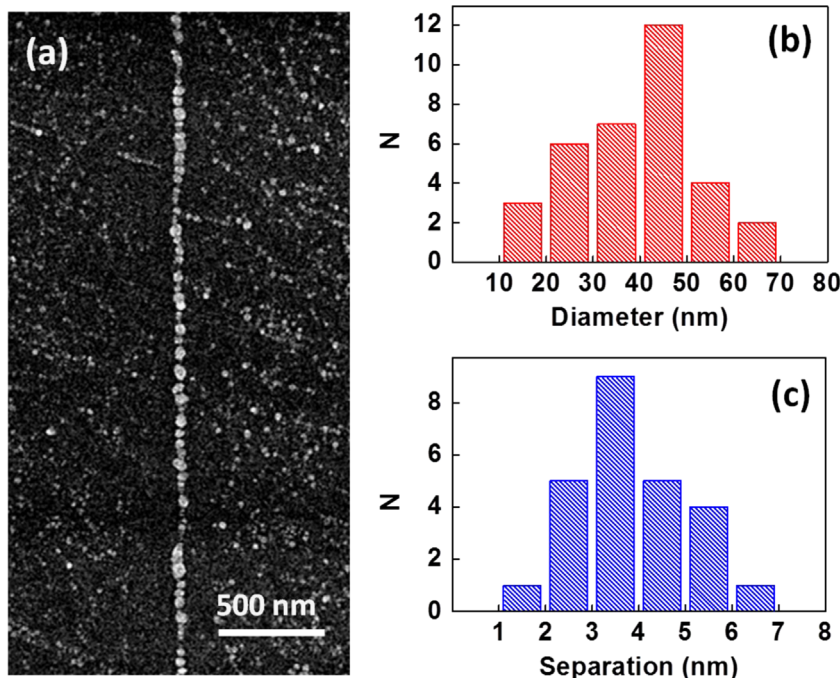


Fig. 1. (a) SEM image of the Y-cut surface of a Nd^{3+} doped PPLN showing a chain of Ag NPs obtained by photochemical procedure on a domain wall surface. (b) Distribution of the NP sizes and (c) inter-particle distances, N being the number of particles.

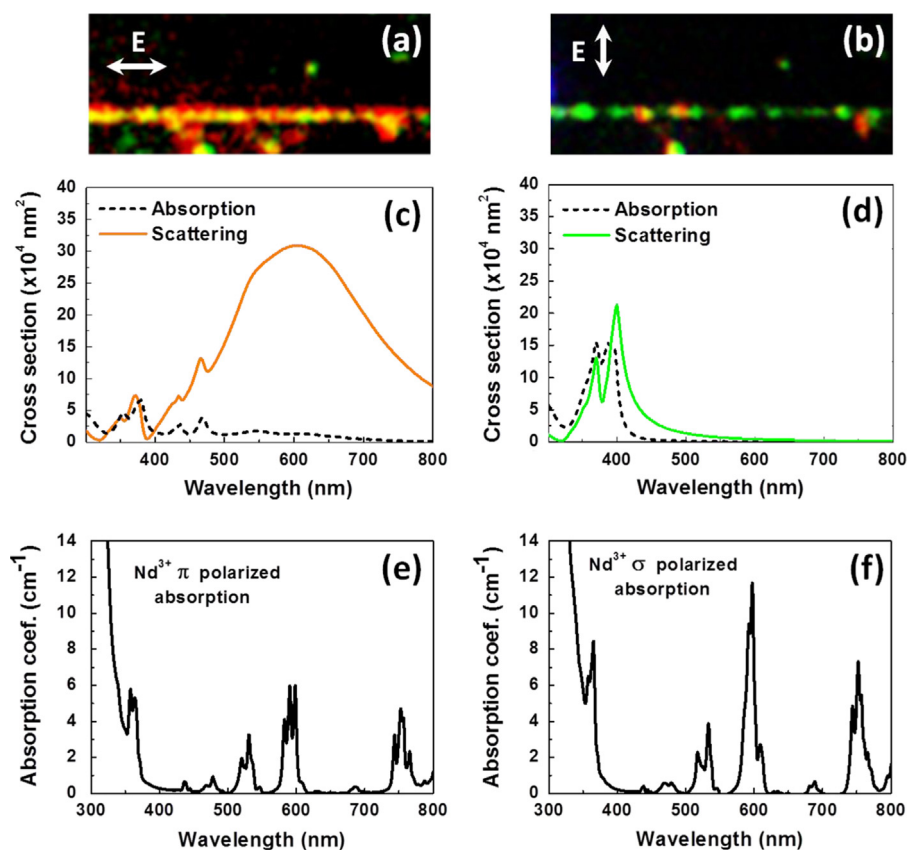


Fig. 3. Dark-field images obtained from a single Ag NP chain for light polarized (a) parallel and (b) perpendicular to the chain axis. Calculated scattering (continuous line) and absorption (dashed line) cross-section spectra of a chain of 15 Ag NPs of 50 nm separated 2 nm for (c) a plane wave polarized parallel to the chain axis and (d) a plane wave polarized perpendicular to the chain axis. (e) and (f) Nd^{3+} absorption spectra corresponding to the π and σ polarized configurations, respectively.

beam was focused to a spot size less than 1 μm , on the surface of the sample by the objectives from the microscope (100 \times magnification), and the photoluminescence signal from the samples was collected in backscattering geometry with the same objective. The absorption spectra of the $\text{Nd}^{3+}:\text{LiNbO}_3$ crystals were obtained with a Lambda 1050 Perkin Elmer spectrophotometer.

2.3. Calculations

Far-field extinction and absorption spectra have been calculated by solving the Maxwell's equations with use of the boundary-element method (BEM) [9,10]. Within the BEM the different inhomogeneous media are described by abrupt interfaces that separate different media characterized by local dielectric functions. The surface charges and currents induced at the interfaces are solved self consistently through a discretization of the boundaries and subsequent solution of the resulting matrix equations. Electromagnetic field is then calculated in terms of these induced charges and currents. In our systems, full convergence of the results was achieved with use of 2 discretization points per nm at each interface between different materials.

3. Results and discussion

Fig. 1(a) shows a SEM image of the selective deposition of Ag metallic nanoparticles on the surface of a Nd^{3+} doped PPLN-Y cut crystal obtained under the experimental conditions described above. The metallic Ag NPs were preferentially deposited on the surfaces of the 180 $^\circ$ ferroelectric domain walls forming linear chains [8]. Due to the bottom-up character of the photochemical technique, the chains

of NPs display a certain degree of disorder. Fig. 1(b) shows the size distribution of the NPs in the chains. As seen, the NPs size ranges from 10 to 70 nm with a maximum at around 40–50 nm. On the other hand, the inter-particle separation varies from 1 to 7 nm showing the most frequent values at around 3–4 nm (Fig. 1(c)).

Varying the number of interacting particles, their average size or their inter-particle separation may affect the localized surface plasmon resonances [11–13]. Therefore, the effects of the particle size distribution and separation distances have been analyzed for our particular system. Fig. 2(a) shows the far field extinction cross-section spectra calculated for different finite chains formed by 15 Ag NPs with particle size of 50 nm (blue line), 15 Ag NPs with particle size of 70 nm (red line) and a mixed chain formed by 6 NPs of 70 nm and 9 NPs of 50 nm (black). The calculations were performed by considering spherical Ag NPs with interspacing distances of 5 nm, as representative values for the interaction. The polarization of the plane wave was parallel to the chain. The position of the main mode converges for chains of about 15 particles, therefore the calculation was limited to that number of particles. The obtained results reveal a red shift of the plasmonic resonance when the size of the silver NPs is increased. In particular, the main mode shifts from 460 nm to 560 nm when the size is increased from 50 nm to 70 nm. On the other hand, mixing NPs of different sizes results into modes located at intermediate wavelengths. Therefore, the size dispersion effects found in our system can be well modeled by simply considering a chain of spheres with a size corresponding to the average size of the distribution (~ 50 nm). The effect of varying the distance between interacting silver NPs is displayed in Fig. 2(b). As observed, decreasing the interspace distance between metallic NPs in a linear chain shifts the maximum of the extinction towards

longer wavelengths due to the increased inter-particle capacitive coupling as the separation distance decreases [14].

To get experimental evidence of the radiative properties of the plasmonic modes supported by the linear chains of Ag NPs deposited on the domain wall surfaces of $\text{Nd}^{3+}:\text{LiNbO}_3$ system dark field microscopy has been used. Fig. 3(a) and (b) show the images corresponding to the visible scattered light obtained from a single chain of Ag NPs for longitudinal and transverse polarizations, respectively. A dominant orange-yellowish color is obtained for light polarized parallel to the chain (Fig. 3(a)). On the other hand, at the same spatial location the scattered radiation switches to green color for light polarized perpendicular to the chain (Fig. 3(b)). These results are compared with the calculated scattering cross-section spectra. Fig. 3(c) and (d) show the polarization of the modes calculated for a finite chain of 15 Ag nanospheres with mixed sizes and 2 nm inter-space distance, as representative values of the

inter-particle interactions. As observed, the spectral differences obtained for the longitudinal and transverse configurations are in good agreement with the experimental dark field images. Specifically, an intense and broad mode with a dominant radiative character is obtained in the range of 500–700 nm for the parallel configuration (Fig. 3(c)), being the corresponding absorption (dashed black spectrum) considerably smaller. For the perpendicular configuration, a small contribution dominates the scattering spectrum in the 450–550 nm range associated with the excitation of the transverse modes of the individual particles, which explains the green scattering seen in the dark field image for this configuration. Here it is important to note that the camera sensitivity favors the green spectral contribution.

Once the spectral features related to the metal Ag NP distribution have been analyzed we consider the effect of the polarization of the spectroscopic properties of Nd^{3+} ions in LiNbO_3 . As known, LiNbO_3 is

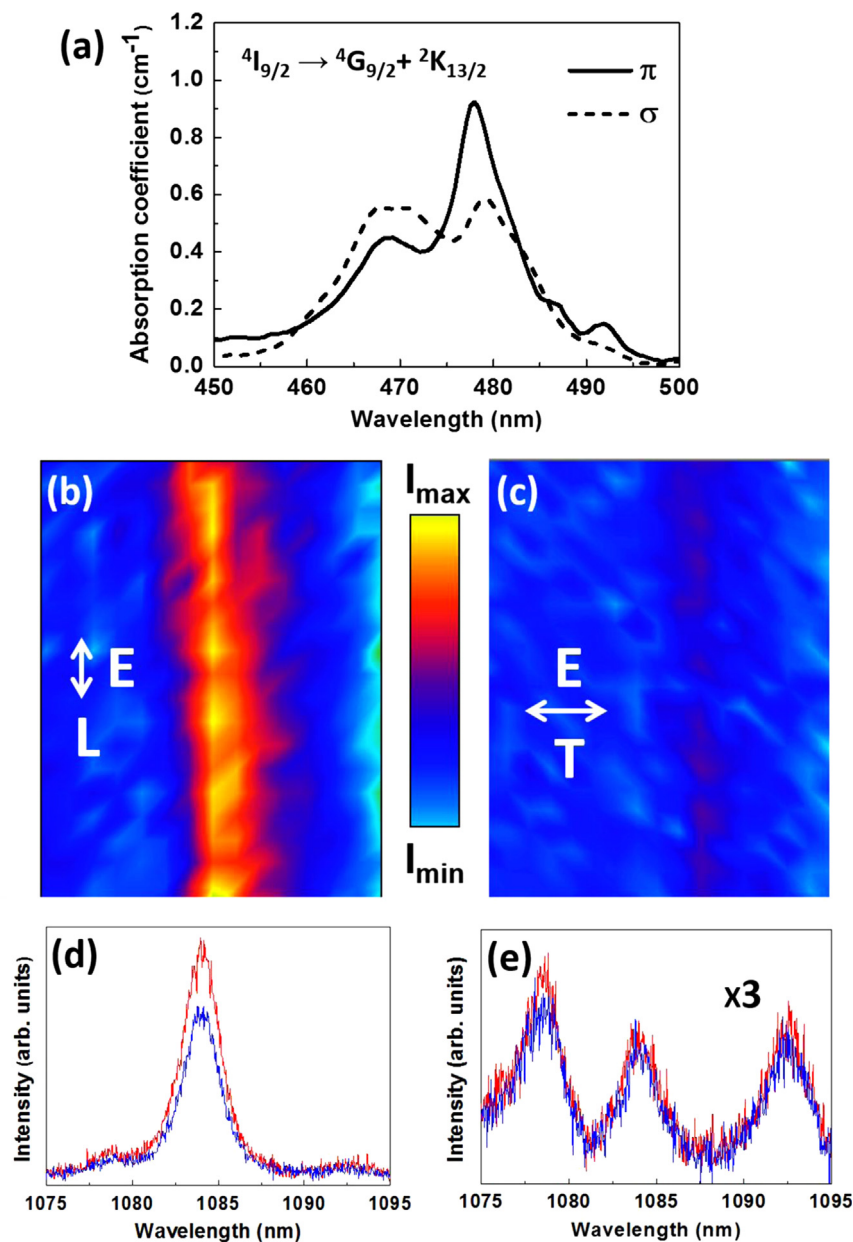


Fig. 4. (a) Absorption spectra of the ${}^4I_{9/2} \rightarrow {}^4G_{9/2} + {}^2K_{13/2}$ transition of Nd^{3+} for π -polarized (continuous) and σ -polarized (dashed) configurations. (b) Micro-fluorescence spatial map of the π -polarized ${}^4F_{3/2} \rightarrow {}^4I_{11/2}$ integrated emission and (c) σ -polarized ${}^4F_{3/2} \rightarrow {}^4I_{11/2}$ emission. (d) π -polarized, and (e) σ -polarized representative emission spectra obtained from the vicinity of the silver nanoparticles chain (red) and from the domain surfaces regions (blue). For interpretation of the references to color in this figure legend, the reader is referred to the web version of this article.

an uniaxial crystal, the symmetry axis being the ferroelectric c -axis. For the Y-cut configuration employed in this work, the ferroelectric c -axis coincides with the axis of the linear chains of Ag NPs. On the other hand, according to the C_3 symmetry site for Nd^{3+} ions in this crystal and to the forced electric-dipole character of the inter-Stark transitions of Nd^{3+} ions in $LiNbO_3$ [15,16], different spectra related to different polarization configurations are obtained. Fig. 3(e) and (f) show the π and σ polarized absorption spectra of Nd^{3+} ions in $LiNbO_3$ in the UV–VIS spectral range obtained before the metallic photo-deposition process. The π (σ) spectrum corresponds to the configuration in which the electric field of the incident light is parallel (perpendicular) to the crystallographic c -axis of $LiNbO_3$. Both spectra display the optical transitions from the $^4I_{9/2}$ ground state to the different 4G_j , 2K_j , $^2P_{1/2}$ and 4D_j excited states of the 4f configuration of Nd^{3+} ions [17]. The relative contribution observed for the different transitions is in agreement with the polarization-dependent character of the Stark transitions of Nd^{3+} in $LiNbO_3$. The comparison between the polarized absorption spectra of Nd^{3+} ions and the scattering cross-section spectra of the Ag NPs chains (Fig. 3(c) and (d)) reveals a large spectral overlap for light polarized parallel to the linear Ag NP chains which are distributed along the ferroelectric c -axis of the crystal. This overlap provides an exceptional support for the assessment of the optical properties of the hybrid metal-gain media under different pumping conditions. In addition, exciting the chain with light polarized parallel or perpendicular to its axis could involve a spectral selection of the π or σ character of the Stark transitions of Nd^{3+} ions located in the vicinity of the Ag NPs.

Finally, the influence of the polarization of the plasmon resonance supported by linear chains on the optical properties of Nd^{3+} ions in this solid state gain medium is analyzed. The specific $^4F_{3/2} \rightarrow ^4I_{11/2}$ emission of Nd^{3+} ions was studied using two different polarization configurations: i) both excitation and emission polarized with the electric field parallel to Ag NPs chain axis, which corresponds to π configuration for Nd^{3+} spectra and ii) both excitation and emission polarized with the electric field perpendicular, σ character of Nd^{3+} spectra. The excitation has been carried out at the $^4I_{9/2} \rightarrow ^4G_{9/2} + ^2K_{13/2}$ absorption of Nd^{3+} ions. For this particular transition the absorption coefficient of Nd^{3+} at the excitation wavelength (488 nm) presents almost identical values for both π and σ configurations (see Fig. 4(a)).

Fig. 4(b) displays the micro-fluorescence spatial map obtained around a single chain of Ag NPs by integrating the obtained π spectra related to the $^4F_{3/2} \rightarrow ^4I_{11/2}$ transition of Nd^{3+} ions when both the excitation and emission beams are polarized parallel to the chain axis. As seen, a clear enhancement of the Nd^{3+} fluorescence is observed around the Ag NPs chain. For the same spatial region, the micro-fluorescence map obtained by integrating the σ spectra for excitation and emission beams polarized perpendicular to the Ag NPs chains is shown in Fig. 4(c). In this case the fluorescence map reveals a very slight enhancement of the Nd^{3+} emission in the vicinity of the Ag NPs. Representative emission spectra collected in and out the vicinity of the Ag NPs chains are displayed in Fig. 4(d) and (e) for the π and σ configurations, respectively. The spectra display a clear structure due to the Stark splitting of the spin-orbit states by the effect of the host crystal field. The number of Stark transitions and their relative intensity are in agreement with the electric-dipole character of the Nd^{3+} Stark transitions and the noninversion C_3 local symmetry site of Nd^{3+} ions in $LiNbO_3$. Moreover, the shape of the Nd^{3+} emission spectra is not modified by the Ag NPs distribution, which indicates that the electric dipole character of the involved Nd^{3+} Stark transitions is not altered by the interaction with the metallic nanostructure. As observed, the dominant effect of the Ag NPs chains consists on the selective enhancement of the specific π main emission line centered at 1085 nm ($R_1 \rightarrow Y_2$) for which laser action has been reported [4]. According to the results of the calculations shown in Fig. 3, the

overlap between the Nd^{3+} absorption transitions and the large main mode of the Ag NPs chains in the longitudinal configuration is a cause responsible for the polarization-selective enhancement of the Nd^{3+} emission. Thus, the near field confinement originated due to the radiative character of the chain mode for light polarized parallel to the chain axis produces the intensification of the absorbed light, and therefore, of the emitted light. Due to the crystal symmetry of the $LiNbO_3$ and to the electric dipole selection rules affecting the $^4F_{3/2} \rightarrow ^4I_{11/2}$ inter-Stark transitions, the intensification of the absorbed light produces, in addition, a spectral selective enhancement of the main laser Stark transition at 1085 nm.

4. Conclusions

We have shown and analyzed the possibility of controlling the optical properties of Nd^{3+} ions by using the polarization features of plasmon modes supported by linear chains of Ag NPs deposited on anisotropic host crystals. In the particular case of Nd^{3+} doped $LiNbO_3$, exciting radiative modes of silver NPs chains with light polarized parallel to their axis produces a spectral-selective intensification of the π -character Stark transitions of Nd^{3+} located in the vicinity of the Ag NPs. The results are relevant to the design of devices for coherent generation at the nanoscale based on rare earth solid state gain media.

Acknowledgments

This work has been supported by the Spanish Ministry of Economy and Competitiveness (MINECO) under projects MAT2010-17443 and MAT2013-43301-R and Comunidad Autónoma de Madrid under project S2013/MIT-2740. MOR acknowledges Ramon y Cajal Contract from Spanish MINECO. LSG acknowledges FPU13/02476 grant from the Spanish Ministry of Education. CT and JA acknowledge financial support from Project FIS2013-41184-P of the Spanish Ministry of Economy and Competitiveness (MINECO), project ETOR-TEK 2014-15 of the Department of Industry of the Basque Government, and from the Department of Education of the Basque Government, IT756-13 of consolidated groups.

References

- [1] L. Novotny, N. van Hulst, *Nat. Photonics* 5 (2011) 83.
- [2] D.K. Gramotnev, S.I. Bozhevolnyi, *Nat. Photonics* 4 (2010) 83.
- [3] M.L. Debasu, D. Ananias, I. Pastoriza-Santos, L.M. Liz-Marzan, J. Rocha, L.D. Carlos, *Adv. Mater.* 25 (2013) 4868.
- [4] T.Y. Fan, A. Cordova-Plaza, M.J.F. Digonnet, R.L. Byer, H.J. Shaw, *J. Opt. Soc. Am. B-Opt. Phys.* 3 (1986) 140.
- [5] Y. Sun, B.S. Eller, R.J. Nemanich, *J. Appl. Phys.* 110 (2011) 084303.
- [6] Y. Sun, R.J. Nemanich, *J. Appl. Phys.* 109 (2011) 104302.
- [7] E. Yraola, P. Molina, J.L. Plaza, M.O. Ramirez, L.E. Bausa, *Adv. Mater.* 25 (2013) 910.
- [8] P. Molina, E. Yraola, M.O. Ramirez, J.L. Plaza, C. de las Heras, L.E. Bausa, *Nano Lett.* 13 (2013) 4931.
- [9] F.J.G. de Abajo, J. Aizpurua, *Phys. Rev. B* 56 (1997) 15873.
- [10] F.J. Garcia de Abajo, A. Howie, *Phys. Rev. Lett.* 80 (1998) 5180.
- [11] R. Esteban, R.W. Taylor, J.J. Baumberg, J. Aizpurua, *Langmuir* 28 (2012) 888.
- [12] C. Tserkezis, R.W. Taylor, J. Beitner, R. Esteban, J.J. Baumberg, *J. Aizpurua, Part. Syst. Charact.* 31 (2014) 152.
- [13] S.T. Jones, R.W. Taylor, R. Esteban, E.K. Abo-Hamed, P.H.H. Bomans, N.A.J. M. Sommerdijk, J. Aizpurua, J.J. Baumberg, O.A. Scherman, *Small* 10 (2014) 4298.
- [14] I. Romero, J. Aizpurua, G.W. Bryant, F.J. Garcia de Abajo, *Opt. Express* 14 (2006) 9988.
- [15] G. Lifante, F. Cusso, F. Jaque, J.A. Sanz-Garcia, A. Monteil, B. Varrel, G. Boulon, J. Garcia Sole, *Chem. Phys. Lett.* 176 (1991) 482.
- [16] R. Burlot, R. Moncorge, H. Manaa, G. Boulon, Y. Guyot, J.G. Sole, D. Cochet Muchy, *Opt. Mater.* 6 (1996) 313.
- [17] H. Loro, M. Voda, F. Jaque, J.G. Sole, J.E.M. Santiuste, *J. Appl. Phys.* 77 (1995) 5929.